Annals of Anatomy 256 (2024) 152312



Contents lists available at ScienceDirect

Annals of Anatomy

journal homepage: www.elsevier.com/locate/aanat

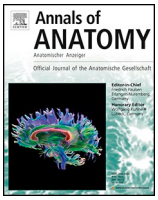



A single Angiofil-latex injection for both radiological and anatomical assessment of arterial territories in the limbs

Julie Manon [a,b,c,*,1], Gaspary Fodjeu [d,e], Robin Evrard [a,b,c], Lucien Van den Broeck [e], Mathieu Jacob [e], Emmanuel Coche [f], Olivier Cornu [a,b,c], Catherine Behets [e,2], Benoît Lengelé [e,g,2]

[a] Université Catholique de Louvain (UCLouvain) – Institut de Recherche Expérimentale et Clinique (IREC), Neuromusculoskeletal Lab (NMSK), Avenue Emmanuel Mounier 53 - B1.53.07, Brussels 1200, Belgium
[b] Cliniques universitaires Saint-Luc, Department of Orthopaedic and Trauma Surgery, Brussels 1200, Belgium
[c] Cliniques universitaires Saint-Luc, Department of Cell and Tissue Therapy, Brussels 1200, Belgium
[d] Université de Yaoundé 1, Cameroon
[e] UCLouvain - IREC, Morphology lab (MORF), Avenue Emmanuel Mounier 52 - B1.52.04, Brussels 1200, Belgium
[f] Cliniques Universitaires Saint-Luc, Department of Radiology, Brussels 1200, Belgium
[g] Cliniques universitaires Saint-Luc, Department of Plastic and Reconstructive Surgery, Brussels 1200, Belgium

ARTICLE INFO

Keywords:
Vascular injection
Angiofil
Contrast agent
Latex
Cast
Computed tomography
Dissection

ABSTRACT

Introduction: Postmortem evaluation of the human vascular system has a long history, with advancements ranging from dissections to modern imaging techniques like computed tomography (CT scan). This study designs a novel combination of Angiofil, a liquid radiopaque polymer, and latex, a flexible cast material, for cadaveric vascular analysis.
Material & methods: The aim was to synergize the advantages of both components, providing accurate radiological images and optimal dissection conditions. Three arterial territories (lateral circumflex femoral artery, profunda brachii artery, and radial artery) were injected and assessed through CT scans and dissections.
Results: The Angiofil-latex mixture allowed successful visualization of the vascular networks, offering a simple, reproducible, and non-toxic approach. Quantitative assessments of the three territories, including diameters and lengths, showed comparable results between CT scan and dissection.
Discussion: The technique precision and versatility make it an accessible and valuable tool for anatomical studies, potentially extending its application to MRI analyses. Overall, the Angiofil-latex combination presents a cost-effective solution for researchers, offering enhanced visibility and detailed anatomical insights for various applications, including anatomical variation studies.

1. Introduction

The human vascular system has been studied postmortem for centuries. The precise description of its anatomy, including its variations, is crucial for further use in education, pathology, forensic medicine, or surgical planning, such as in vascularized flap reconstructions (Grabherr et al., 2007; Renard et al., 2018). During the 16th century, Andreas Vesalius and Leonardo da Vinci laid the foundation for human vascular anatomy through extensive dissections of cadavers (Salmon, 1936; Taylor and Pan, 1998; Bergeron et al., 2006; Grabherr et al., 2007; Taylor et al., 2017; Renard et al., 2018). Over the years, numerous intravascular injection techniques have been reported, varying from different liquid-colored dyes to wax casts (fluid that solidifies intravascularly) and increasing the visibility of blood vessels during dissection (Bergeron et al., 2006; Grabherr et al., 2007; Jackowski et al., 2008; Evrard et al., 2024). The development of X-rays and computed tomography (CT scan) allowed to study human vascular system more extensively in a less invasive way thanks to the injection of radiopaque

* Corresponding author at: Université Catholique de Louvain (UCLouvain) – Institut de Recherche Expérimentale et Clinique (IREC), Neuromusculoskeletal Lab (NMSK), Avenue Emmanuel Mounier 53 - B1.53.07, Brussels 1200, Belgium.
E-mail address: julie.manon@uclouvain.be (J. Manon).
[1] ORCID number: 0000–0002-2558–8723
[2] *Authors share the last authorship; they contributed equally to this work.*

https://doi.org/10.1016/j.aanat.2024.152312
Received 29 May 2024; Received in revised form 29 June 2024; Accepted 21 July 2024
Available online 25 July 2024
0940-9602/© 2024 The Authors. Published by Elsevier GmbH. This is an open access article under the CC BY-NC-ND license (http://creativecommons.org/licenses/by-nc-nd/4.0/).

contrast agents, such as barium, lead oxide, or iodine (Bergeron et al., 2006; Grabherr et al., 2014; Renard et al., 2018), even if dissection, direct visualization, and conventional autopsy remained the gold standards (Chevallier et al., 2013).

Nowadays, contrast agents and vascular cast materials remain commonly used in postmortem evaluation of vascular anatomy, but separately. Both techniques have advantages and limitations. Studies using contrast agents are typically non-invasive. Most of them are used efficiently *in vivo*, in the diagnosis of vascular diseases or preoperative planning (Renard et al., 2018). The main limitations are the agent penetration, the machine resolution, and the allergic reaction risk (Boyd et al., 2017; Bruen et al., 2022; Rosado Ingelmo et al., 2016). On the other hand, postmortem injection of colored casting material provides a detailed 3D view of the vascular tree, including anatomical variations and relationship to other soft tissues or solid organs that are not visible under X-ray. However, this technique is invasive and restricted to cadavers, limiting its use to research, forensic medicine, and educational purposes. Its resolution depends on the degree of penetration and the dissection precision.

Nevertheless, a good mixture for cadaveric vascular studies might combine a suitable radiologic contrast, a colored macroscopic appearance facilitating the identification of vessels, and a proper solidification over time giving sufficient elasticity for vascular dissections and measurements (Renard et al., 2018). Among the various substances available, Angiofil and latex have garnered attention for their unique properties and applications.

Angiofil is a radiopaque liquid polymer based on lipophilic iodine that offers excellent radiological visibility due to its adjustable viscosity and the absence of sedimentation (Grabherr et al., 2008a). As an oily contrast agent (Chevallier et al., 2013), it has the advantage of its intravascular retention for days after injection without any extravasation (a, 2008, 2008b, 2007; Renard et al., 2018). Moreover, histological analyses are not influenced by its injection (Stumm et al., 2020).

Latex is a flexible and resilient cast material that visually guides the gross dissection while preserving vessel integrity thanks to its elasticity (Bergeron et al., 2006; Fonkoue et al., 2021; Renard et al., 2018). When injected into blood vessels, latex hardens, creating a 3D replica of the vascular system. With the addition of a few drops of dye, it provides an excellent macroscopic visibility greatly facilitating meticulous dissection (Fonkoue et al., 2021). Its manipulation is easy and leads to reproducible results (Renard et al., 2018). Delayed analyses are possible thanks to the rigid intravascular moulding. Since pre-vulcanized stabilized with ammonia, the latex might also be used as a suspending medium for lipophilic radiopaque agents (Bergeron et al., 2006). To our knowledge, both these compounds have not yet been associated in a single intravascular injection.

The aim of this study was to develop a simple, cheap, reproducible, and non-toxic mixture of Angiofil and latex for cadaveric anatomical analysis of arteries of the upper and lower limbs. To synergize the advantages of Angiofil and latex in a single vascular injection could lead to a robust methodology that goes beyond the limitations of individual techniques. This research evaluates if this combination could provide both accurate radiological images and optimal dissection under facilitated conditions, from a qualitative and a quantitative point of view.

2. Material & methods

2.1. Human specimens and arterial territories

Human cadaveric donors were received from the Human Anatomy Department of UCLouvain (IRB00008535, Brussels, Belgium). Distinct limbs were harvested for each vascular territory, following local ethics committee authorization (Ref 2021–30AOU-356, approved on the 13th of September 2021). Respective limbs were cut and immediately fresh-frozen within 24–36 hours of death. Three vascular territories were assessed, namely the lateral circumflex femoral artery (LCFA), the profunda brachii artery (PBA), and the radial artery (RA). Demographics of each specimen set are collected in Table 1.

The limbs were thawed upside down to bleed out at room temperature (RT) for at least 24 hours. The upper limbs were hung by the fifth finger and the lower limbs by the hallux. The blood leaving the vascular system was collected including blood liquid and clots to approximate the fluid volume to be injected next. The physical integrity of the limbs was also inspected (skin aspect, existence of possible lesions, bruises, scars, or other variants of normality).

2.2. Rinse

All the following steps were performed with the limb lying on a dissection table. Each specimen was rinsed through a main artery upstream of the artery of interest in order to keep the latter as intact as possible and prevent the leakage of rinse or injection. A minimal dissection was made from the proximal extremity of lower and upper limbs to identify the arterial bifurcation between the femoral artery (FA) and the profunda femoris artery (PFA), and between the brachial artery (BA) and the PBA, respectively. In the limbs reserved for analysis of RA territory, a minimal skin incision was made medially to the biceps brachii tendon in order to locate and dissect the BA.

Each main artery (FA and BA) was cut to insert a metal rinsing cannula, which was clamped to ensure an airtight connection. The cannula was connected with a purged plastic tube to a glass jar filled with 0.9 % NaCl solution preheated to 56°C. Subsequently, a pump permitted to circulate (max speed: 30 rpm) 400 mL, 1 L, and 2 L of physiological fluid through the arterial network to fully rinse it, for the RA, PBA, and LCFA territories, respectively. The clearing of the venous outflow attested the efficacy of the rinse. Attention was paid to possible swelling of soft tissues.

2.3. Angiofil-latex injection

Preliminary tests were conducted on extra specimens (details not reported in this study) to adjust the Angiofil concentration in the mixture and identify potential pitfalls during the establishment of the technique. The preliminary results, which were used to establish the systematic approach of the technique, were not considered in this study.

The injection was performed into the arteries of interest, namely the LCFA, the PBA, and the RA. Their dissection was carried out carefully in order to avoid cutting small collaterals, as well as leakage and accumulation of mixture outside the vascular tree for cleaner radiological and anatomical images.

The LCFA and the PBA were dissected anterogradely. For the RA, a second cutaneous incision was made in the forearm, following a volar Henry's approach (Catalano et al., 2011; Protopsaltis and Ruch, 2008). The incision started at the distal forearm, between the styloid process of the radius and the flexor carpi radialis tendon. It was extended proximally in the distal third of the forearm, towards the trochlea of the humerus.

After locating and dissecting the artery of interest, a catheter

Table 1
Demographics of each set of five samples for each vascular territory.

	Number of limbs	*Number of donors*	*Sex*	*Age (mean +/- SD)*	*Laterality*
LCFA	5	4	3 ♂ / 1 ♀	73.3 +/- 19.1	4 L / 1 R
PBA	5	4	2 ♂ / 2 ♀	73.2 +/- 9.3	4 L / 1 R
RA	5	4	2 ♂ / 2 ♀	82.1 +/- 13.5	2 L / 3 R

SD: standard deviation, LCFA: lateral circumflex femoral artery, PBA: profunda brachii artery, RA: radial artery, ♂: men, ♀: women, L: left, R: right.

(14–22 G, depending on the diameter of the artery, Terumo, Versatus-W) was inserted and fixed with surgical thread (Surgilon™ 2.0). A mixture of latex (Latex "LA", with 0.38 % ammoniac, 603, Finres) added with a 20 % volume of liposoluble iodine-based agent (Angiofil, S500.0028, Fumedica AG, Switzerland) (1:5 mixture Angiofil: latex, v/v), and a few drops of red dye (Jesmonite, bright red pigment, 200 g, Finres) was prepared and shaken by hand at RT until a homogeneous appearance. The mixture was injected into the artery under continuous manual pressure on the syringe. Several limbs were injected under fluoroscopy to visualize the contrast agent progression, to correlate the manual pressure perceived and arterial filling, and to make sure the vascular system was completely filled. The injection volume was estimated on the venous drainage volume. After the volume was injected, the artery was clamped over the catheter to maintain the fluid pressure, ensuring the dissemination to smaller vessels, and avoiding any reflux.

2.4. Angioscanner

The injected limbs were placed in a fully extended position in the CT scan. The various acquisitions were performed on a Somatom Definition AS 128 scanner (Siemens Healthineers, Erlangen, Germany). The acquisitions were conducted in ultra-high-definition mode (beam collimation 0.3 mm, tube voltage 120 kV, tube current 200–250mAs). Subsequently, they were reformed using both hard and soft kernels with a slice thickness of 0.4 mm. Volume rendering, a post-processing technique (Dappa et al., 2016; de Spiegeleire et al., 2019), allowed reconstructions and complex anatomical analyses, using the Syngo.Via tool in cinematic rendering mode. This step was performed the same day as the vascular injection or the next one, as the Angiofil-latex mixture does not need to be solidified to visualize its route. However, for the next step (dissection), it was primordial to place the limb in a cold room (4°C) for 72 hours to permit rigidification.

2.5. Dissections

All collateral and terminal branches of the artery of interest were identified. The dissection of the LCFA followed previously established protocols (Saint-Cyr et al., 2012; Lee et al., 2015; Manon et al., 2022, 2023). The skin incision was made 1 cm medially to the standard landmark between the anterior superior iliac spine and the lateral border of the patella (Fig. 1a) in order to preserve the perforator vessels which were further dissected. The descending branch (DB) of the LCFA was always found distally through the intermuscular fascia between the vastus lateralis and the rectus femoris. The LCFA was retrogradely dissected including the DB and the transverse branch (TB) until the PFA proximally, and anterogradely through the vastus lateralis muscle or its fascia until the perforators distally.

The PBA was dissected using a posterior approach of the arm, followed by an anterior approach of the elbow (Fig. 1b). The skin was incised following a line between the humerus surgical neck and the olecranon. The lateral and long heads of the triceps brachii muscle were discarded in order to enter the radial groove. The radial nerve and the PBA were identified and dissected. The proximal humeral insertion of the lateral head of the triceps brachii was cut to highlight all collateral branches of the PBA, *i.e.* the radial collateral artery (RCA) and the medial collateral artery (MCA). To allow a better global view of the ramifications of the PBA, the palmar region of the arm and the elbow was also exposed through a mid-line anterior incision. On the medial side, the superior ulnar collateral artery (SUCA) and inferior ulnar collateral artery (IUCA) were dissected anterogradely from the BA. The bifurcation of the BA into radial and ulnar arteries was identified. Their respective radial recurrent artery (RRA) and ulnar recurrent artery (URA) joined the RCA, MCA, and ulnar collaterals in the articular network of the elbow.

For the RA territory, the dissection began by extending the radial incision distally around the palm until the base of the little finger (Fig. 1c). The first and second fingers were also incised to their tip. The superficial palmar aponeurosis was removed to expose and dissect the

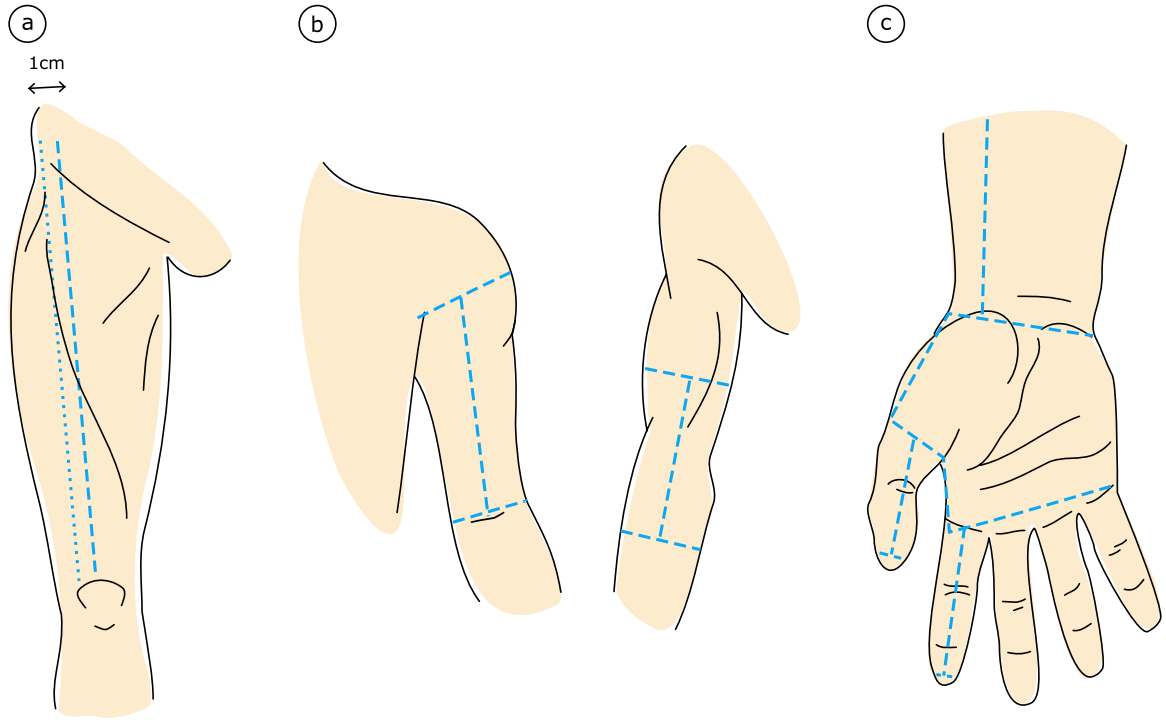

Fig. 1. Landmarks for skin incisions (blue dashed lines) in the corresponding anatomical region, for the lateral circumflex femoral artery (LCFA) territory (a), the profunda brachii artery (PBA) territory (b), and the radial artery (RA) territory dissections (c). The blue dotted line (a) represents the theoretical skin incision to perform an anterolateral thigh flap.

superficial palmar branch (SPB) of the RA, the superficial palmar arch (SPA) and its branches, with a specific focus on the ulnar palmar digital artery of the index (UPDAI). Subsequently, the SPA as well as flexor tendons were transected at the level of the carpal tunnel and retracted upward. The carpometacarpal joint of the thumb (trapezometacarpal joint) was disarticulated to provide clear visibility of the entire course of the RA. Furthermore, the deep palmar arch (DPA) and the palmar arteries of the thumb, namely the radial palmar artery of the thumb (RPDAT) and the ulnar palmar digital artery of the thumb (UPDAT), known to rise from the princeps pollicis artery, were dissected. The first common palmar digital artery (CPDAI), the radialis indicis artery (RIA, synonym of the radial palmar digital artery of the index), and the first (M1), second (M2), and third (M3) palmar metacarpal arteries were also explored.

2.6. Quantitative analyses

In addition to usual qualitative assessment, diameters and lengths of three arterial territories in limbs were quantified and compared. During the dissection, a digital calliper (resolution = 0.01 mm ± 0.03 mm) and a metal ruler were respectively used to measure artery diameters (Ø) at different specific levels (Fig. 2), and the length from their origin to their termination. Globally, the ØLCFA was taken at its origin, as for the ØDB and the ØTB. The ØPBA and collaterals were taken at their origin and their end, assuming to be at the thinnest zone of the anastomosis with respective recurrent arteries. The ØRA was measured at the top of the radial styloid process. The Ø of digital arteries was measured at three locations: the metacarpophalangeal joint (MCP), the proximal interphalangeal joint (PIP), and the distal interphalangeal joint (DIP), or interphalangeal joint (IP) for the thumb.

As for the length of the LCFA vascular tree, the length of perforators was taken. The perforators were classified following the Yu's classification (Yu, 2004). This classification is based on three localizations, *i.e.* A being the most proximal perforators of the thigh, B the middle ones, and C the most distal ones. Two lengths were measured for each perforator, *i.e.* the total length and the perforator length. The total length started from the bifurcation between the PFA and the FA until the location of the perforation of the fascia lata. The perforator length started from the origin of the perforator on its corresponding branch (TB or DB) until the location of the perforation. The RA length was measured from the radial styloid process to the origin of the deep palmar artery (DPA). The length of all the other arteries was measured from their origin to their end.

Concerning the CT scan, all the measurements were taken on a dedicated software (Carestream Health, Vue PACS, v. 12.1.5.5151, Philips Medical Systems, the Netherlands), using the maximum intensity projections (MIP) on multiplanar reconstruction. Diameters and lengths were measured at exactly the same locations as those performed during dissection.

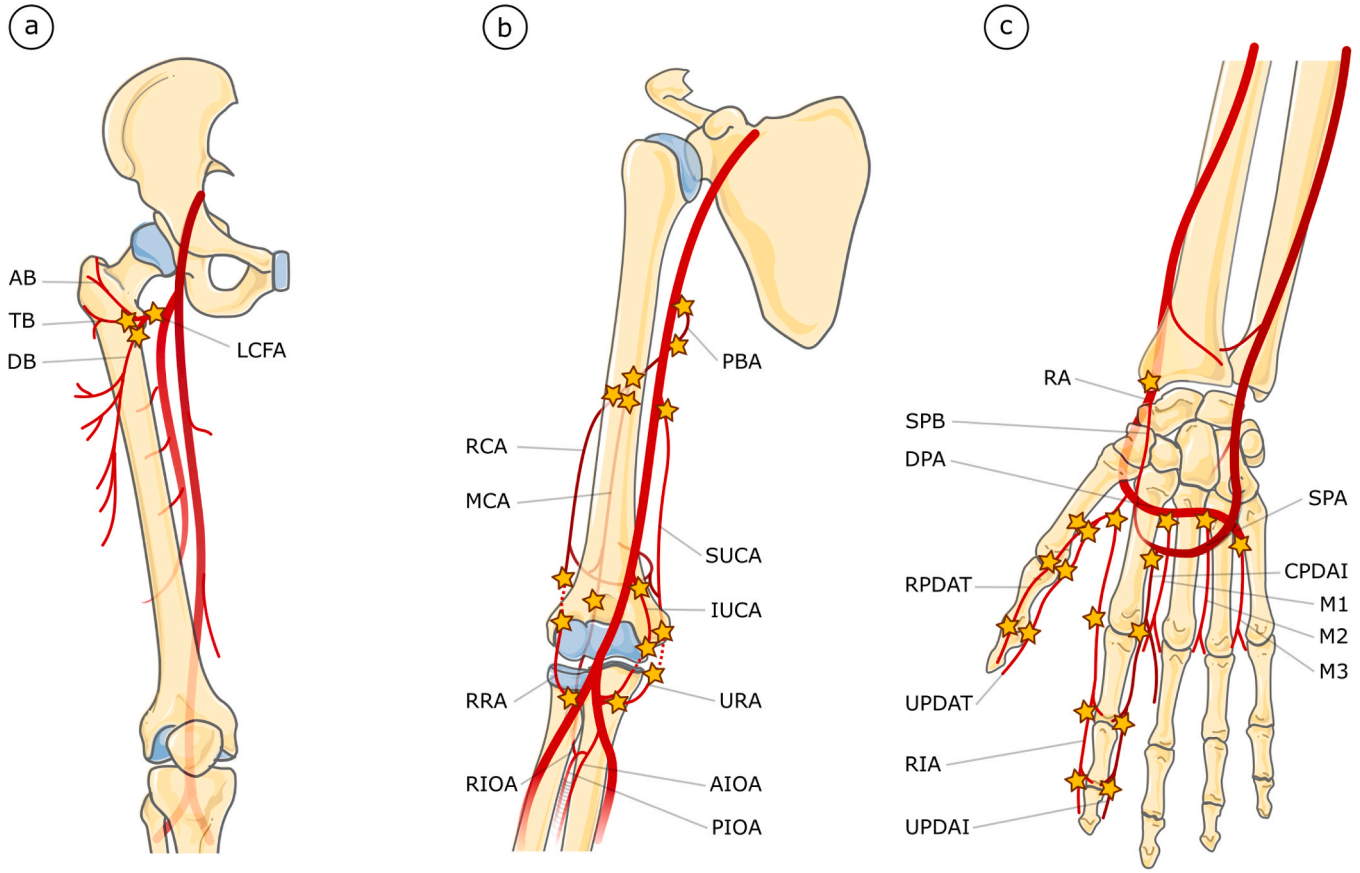

Fig. 2. Location of diameter measurements (yellow stars) in the LCFA territory (a), the PBA territory (b), and the RA territory (c). LCFA: lateral circumflex femoral artery, AB: ascending branch, TB: transverse branch, DB: descending branch, PBA: profunda brachii artery, RCA: radial collateral artery, MCA: medial collateral artery, SUCA: superior ulnar collateral artery, IUCA: inferior ulnar collateral artery, RRA: radial recurrent artery, URA: ulnar recurrent artery, RIOA: recurrent interosseous artery, AIOA: anterior interosseous artery, PIOA: posterior interosseous artery, RA: radial artery, SPB: superficial palmar branch of the RA, DPA: deep palmar arch, RPDAT: radial palmar digital artery of the thumb, UPDAT: ulnar palmar digital artery of the thumb, RIA: radialis indicis artery, UPDAI: ulnar palmar digital artery of the index, SPA: superficial palmar arch, CPDAI: common palmar digital artery of the index, M1: 1st palmar metacarpal artery, M2: 2nd palmar metacarpal artery, M3: 3rd palmar metacarpal artery.

2.7. Statistics

Descriptive analyses first characterized the independent quantitative values. Data were expressed as the mean +/- standard deviation (SD), and/or by boxplots and histograms. Their distribution was assessed by QQ plots and Shapiro-Wilk tests. Since not every distribution was normal and due to the small sample size, nonparametric Wilcoxon paired tests were performed. The level of significance was determined as $p<0.05$. The agreement between measurements obtained from dissection and CT scan was assessed using the Intraclass Correlation Coefficient (ICC). ICC was calculated using a two-way mixed model with absolute agreement, where each measurement was considered a single observation among a larger dataset. All statistics were made using SPSS software (V.27, IBM SPSS, Inc., Chicago, IL, United States).

3. Results

The injected volume of Angiofil-latex ranged from 9 mL to 10 mL (average 9.6 +/- 0.9 mL) for the LCFA, 7 mL to 20 mL (average 13.1 +/- 5.2 mL) for the PBA, 5.5 mL to 10 mL (average 7.5 +/- 1.7 mL) for the RA to fill in the vascular tree. The death-to-perfusion time was 971.4 +/- 1494.8 days.

3.1. Preliminary results

During the establishment of the technique, the main pitfalls were pre-studied and revealed blood clots, leakage, and air bubbles as technique failure (Fig. 3). Blood clots are crenelated in the opposite of air bubbles that are rounded thanks to their surface tension. Blood clots were seen after an insufficient rinse and air bubbles after air injection within the mixture. Leakages usually occurred after a not enough meticulous dissection disrupting small collaterals.

3.2. Qualitative observations

The vascular network of the three arteries of interest was visualized on the CT scan (Fig. 4 – above). For the LCFA territory, both the TB and DB were opacified as well as their ramifications. The FA was not opacified but exhibited many calcifications which have the same density as the Angiofil. The PBA territory also showed a complete filling with a retrograde opacification of the BA territory, including the RA, UA, and the recurrent arteries of the elbow (RRA and URA, respectively). For the RA territory, the opacification went until the small subcutaneous arteries of fingers. The latex was solidified in all specimens and allowed a rigorous dissection thanks to a macroscopic enhancement of the artery visualization (Fig. 4 – below). The protocol also allowed to highlight anastomoses. For example, despite a single injection into the RA, the distal vascular network of the ulnar artery was systematically observed and filled with the Angiofil-latex mixture (Fig. 4c). Furthermore, the combination of Angiofil-latex injection with 3D angioscanner reconstructions also allowed to emphasize, with an increased definition, the numerous perforator vessels supplying the skin territory of the antero-lateral thigh flap (Fig. 4a), the cutaneous area of the lateral arm flap (Fig. 4b), and the skin paddle of the thenar flap, respectively from the LCFA, the PBA and the SPB (Fig. 4c).

The small subcutaneous vessels were properly filled with Angiofil-latex and were visible during fluoroscopy, CT scan, and dissection (Fig. 5). The smallest visualized artery reached the maximal precision permitted by the CT scan resolution (0.3 mm). This resolution however allowed to precisely observe the numerous tiny cutaneous side branches of the palmar digital arteries supporting the blood supply of the Littler's latero-digital flap (Littler, 1953), as well as the pulpar arterial network supplying the Atazoy's pulpar advancement flap (Atasoy et al., 1970).

However, one of the five upper limbs presented a leakage of Angiofil-Latex mixture out of the origin of the PBA. This vascular territory was not correctly opacified and the quantitative analyses were not possible.

This protocol allowed to precisely study individual anatomical variations. As an example, the vascularization of the thumb is classically

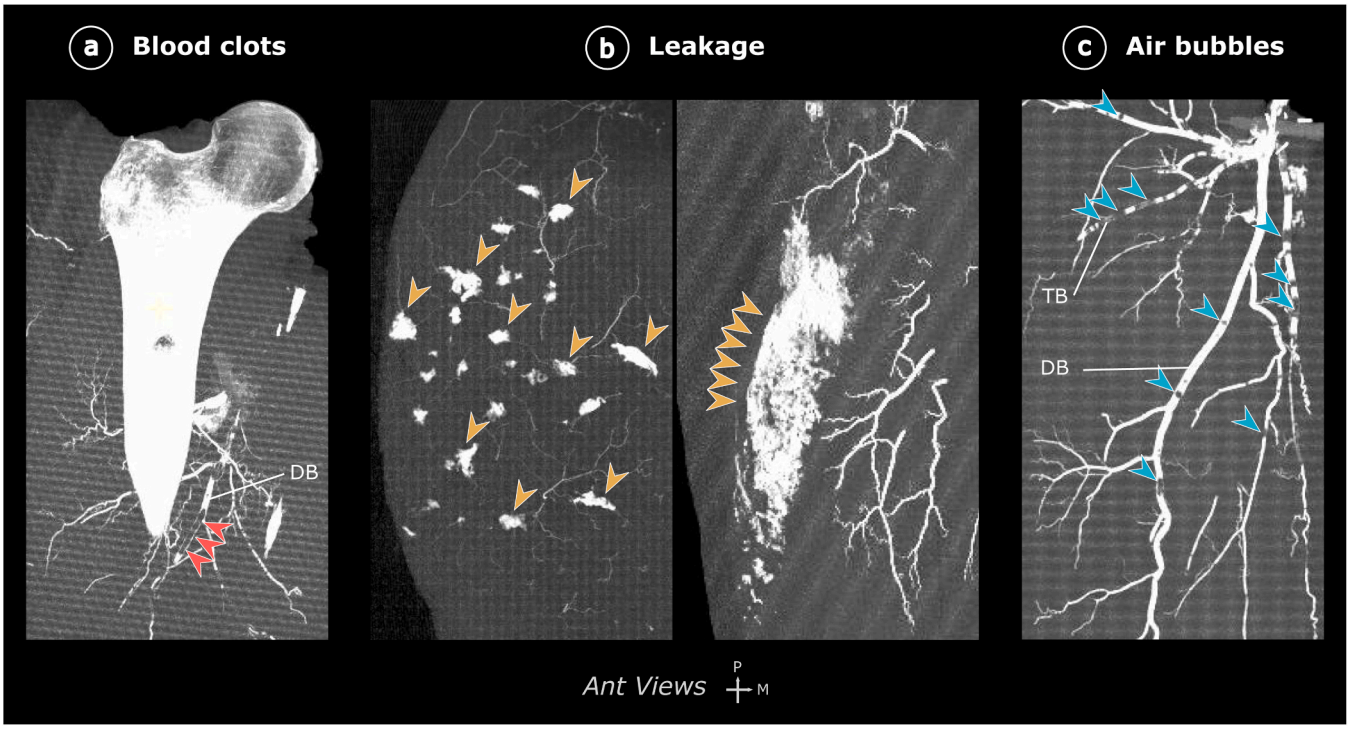

Fig. 3. Injection flaws illustrated by maximum intensity projections (MIP) on the multiplanar reconstruction of the LCFA territory. Defects in injection include residual blood clots (a), contrast agent leakage (b), and injection of air bubbles (c). Leakage can be seen in different planes including in the subcutaneous layer (b – left), or the subfascial compartment (b – right). DB: descending branch, TB: transverse branch, Ant: anterior, P: proximal, M: medial.

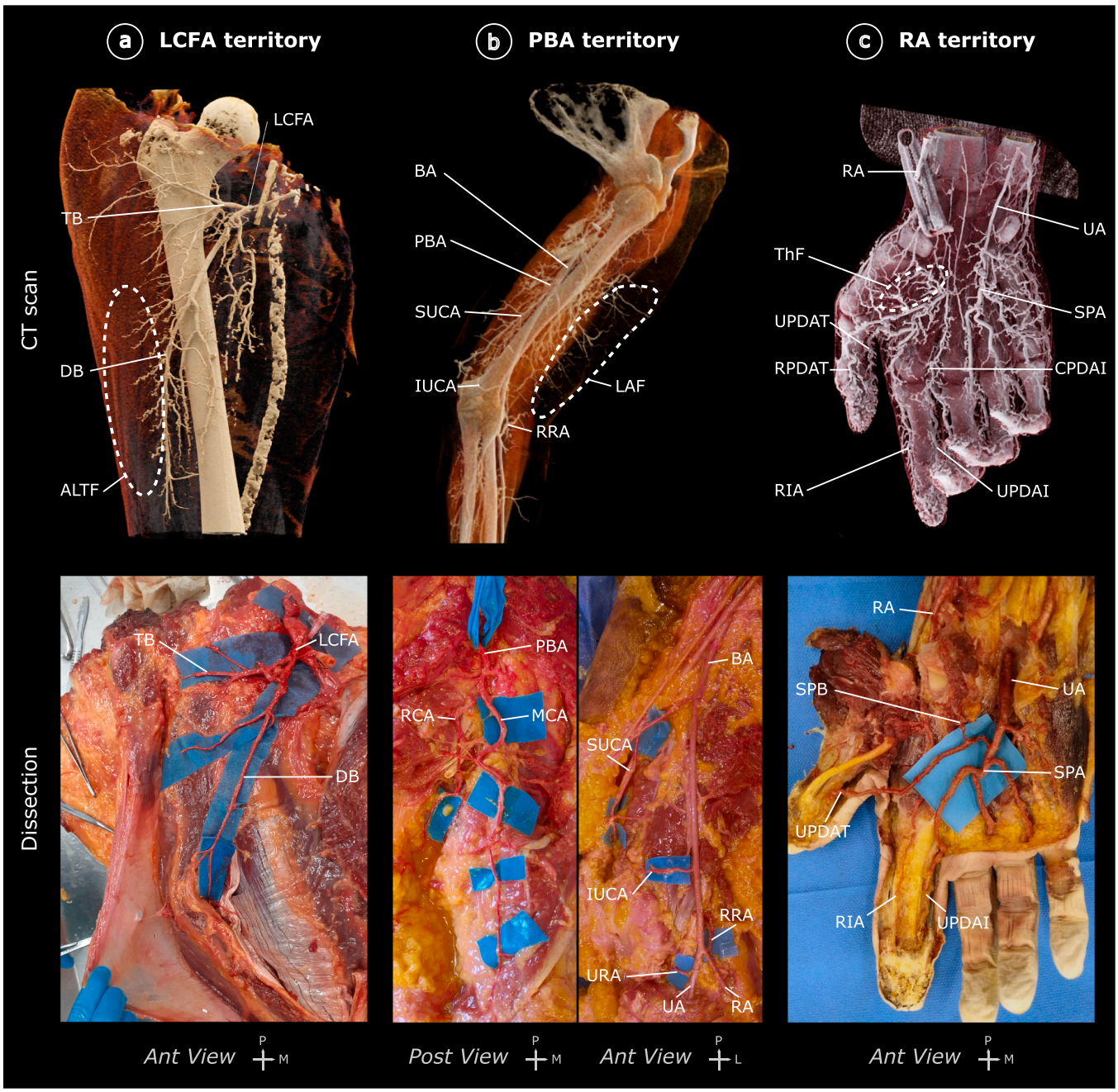

Fig. 4. Visualization of the LCFA territory (a), the PBA territory (b), and the RA territory (c), after 3D reconstructions post-CT scan (above), and after dissection (below). Each sample originated from distinct donors. LCFA: lateral circumflex femoral artery, TB: transverse branch, DB: descending branch, ALTF: anterolateral thigh flap, BA: brachial artery, PBA: profunda brachii artery, RCA: radial collateral artery, MCA: medial collateral artery, SUCA: superior ulnar collateral artery, IUCA: inferior ulnar collateral artery, LAF: lateral arm flap, RRA: radial recurrent artery, URA: ulnar recurrent artery, RA: radial artery, UA: ulnar artery, ThF: thenar flap, UPDAT: ulnar palmar digital artery of the thumb, RPDAT: radial palmar digital artery of the thumb, RIA: radialis indicis artery, UPDAI: ulnar palmar digital artery of the index, CPDAI: common palmar digital artery of the index, SPA: superficial palmar arch, SPB: superficial palmar branch of the RA, Ant: anterior, Post: posterior, P: proximal, L: lateral, M: medial.

described as primarily dependent on the princeps pollicis artery (Miletin et al., 2017; Park et al., 2021). This artery would come from the RA after it crosses the first intermetacarpal space, then move towards the thumb and divide into two palmar digital arteries (UPDAT and RPDAT). In our study, those two branches were identified in each hand. However, out of the five dissected hands, only one exhibited a princeps pollicis artery. In the remaining four hands, UPDAT and RPDAT had different origins from the conventional pattern (Table 2).

3.3. Diameters of arteries

Angiofil-latex injection enabled to fill arteries of many different diameters from the larger one in the LCFA (ØLCFA = 6.40 +/- 1.66 mm) to the smallest ones in the RPDAT at the IP joint (ØRPDAT = 0.53 +/- 0.06 mm) or the RIA at the DIP joint (ØRIA = 0.53 +/- 0.11 mm). The diameter consistently decreased as the artery progressed distally (*e.g.* $ØRPDAT_{origin}$ = 1.13 +/- 0.20 mm, $ØRPDAT_{IP}$ = 0.53 +/- 0.06 mm), or from a proximal artery to a more distal one (*e.g.* ØLCFA = 6.40 +/- 1.66 mm, ØDB = 4.27 +/- 0.92 mm). Even after dissection, this

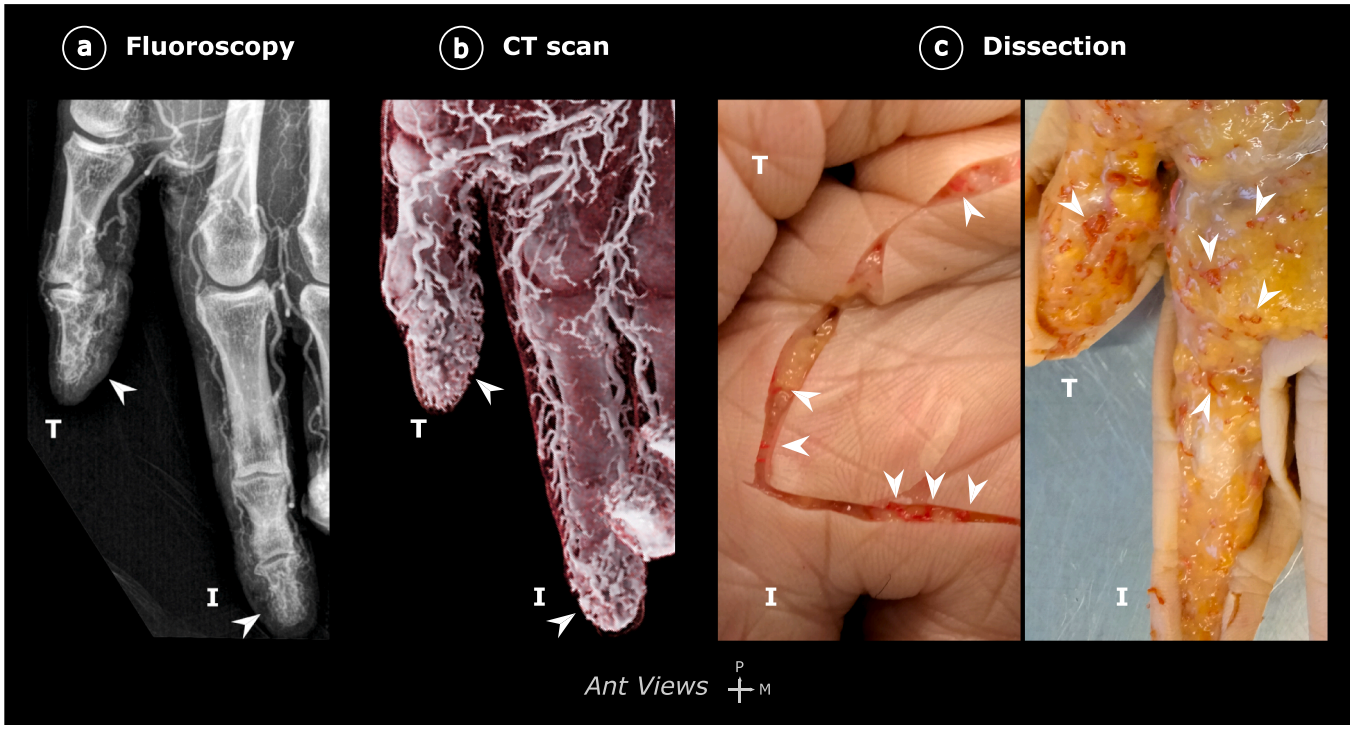

Fig. 5. Visualization of the small subcutaneous arteries (white arrowheads) of the thumb and the index, filled with Angiofil-latex on fluoroscopy (a), CT scan (b), and dissection (c). T: thumb, I: index, Ant: anterior, P: proximal, M: medial.

Table 2
Origin of the two palmar digital arteries of the thumb.

Subjects	Origin of UPDAT	Origin of RPDAT
1	Deep palmar arch	Radial artery (palmar superficial branch)
2	Superficial palmar arch	Radial artery
3	Superficial palmar arch	Radial artery
4	Deep palmar arch	Radial artery (palmar superficial branch)
5	Princeps pollicis artery	

UPDAT: ulnar palmar digital artery of the thumb, RPDAT: radial palmar digital artery of the thumb.

observation was similar to that of the CT scan (Fig. 6). On the contrary, arteries of the same level have the same diameters (*e.g.* ØMCA = 1.40 +/- 0.29 mm, ØRCA = 1.45 +/- 0.29 mm).

However, even if the central tendencies (means and medians) seem often higher on the CT scan than on dissection (*e.g.* mean $ØM1_{CT\ scan}$ = 1.09 +/- 0.23 mm and mean $ØM1_{dissection}$ = 0.92 +/- 0.27 mm respectively), statistical difference was not often observed between both techniques (Additional Table A). The variabilities of the data were also similar between CT scan and dissection measures. This point is illustrated by the height of the boxplot in Fig. 6 (and the SD in Additional Table A). This suggests that the dispersion of the measured values remains consistent between the two groups. The ICC was 0.978 (IC95 % 0.964 – 0.986), which indicates highly consistent and reliable methods.

3.4. Length of arteries

Most of the data were not significantly different between both techniques (Fig. 7). Only the total length of B perforators (dissection = 18.4 +/- 4.1 cm, CT scan = 16.3 +/- 3.8 cm), RA (dissection = 6.24 +/- 0.21 cm, CT scan = 6.56 +/- 0.25 cm), UPDAT (dissection = 9.60 +/- 2.29 cm, CT scan = 10.33 +/- 2.90 cm), and RIA (dissection = 12.64 +/- 0.84 cm, CT scan = 13.56 +/- 1.17 cm) were significantly different when measured on dissection or CT scan ($p<0.05$).

The same observation was made for the length as for the diameter concerning the variabilities of the data. Once again, the similarity was influenced more by the artery itself than by the technique used. This point is illustrated by the error bars in Fig. 7 (and the SD in Additional Table B).

The overall ICC between both methods was 0.952 (IC95 % 0.934 – 0.965), which indicates highly consistent and reliable methods, as for the diameter.

4. Discussion

Qualitatively, the single Angiofil-latex injection allowed to clearly visualize the network of the injected arteries in both CT scan and dissection. CT scan images and 3D reconstructions demonstrated remarkable precision in visualizing the vascular anatomy of small arteries, reaching the maximal precision of the machine (0.3 mm). The three vascular territories included arteries of different diameters and lengths revealing a homogeneous success of the technique. The larger trunks were full and expanded, the anastomoses were filled, and the tiny subcutaneous arterioles of the fingers were visualized.

4.1. Diameter and length comparison

Dissection and CT scan measurements of the diameter and the length were comparable for most of the arteries, with excellent consistency and reliability.

Concerning the diameter, when a significant difference existed, the CT scan diameter was always larger than in dissection. The use of Angiofil may cause an exaggeration of diameters owing to its high concentration and potential overexposure. The adjustment of brightness and contrast of the CT scan needs to be used carefully in order not to create bias in measurements. On the opposite, the use of cast material can sometimes create shrinkage after solidification (Grabherr et al., 2007), which can be counterbalanced by the good elasticity of the latex. The use of a calliper during dissections might also slightly compress the vessels, according to the latex elasticity, artificially reducing diameters. However, most of the measurements were not affected by the

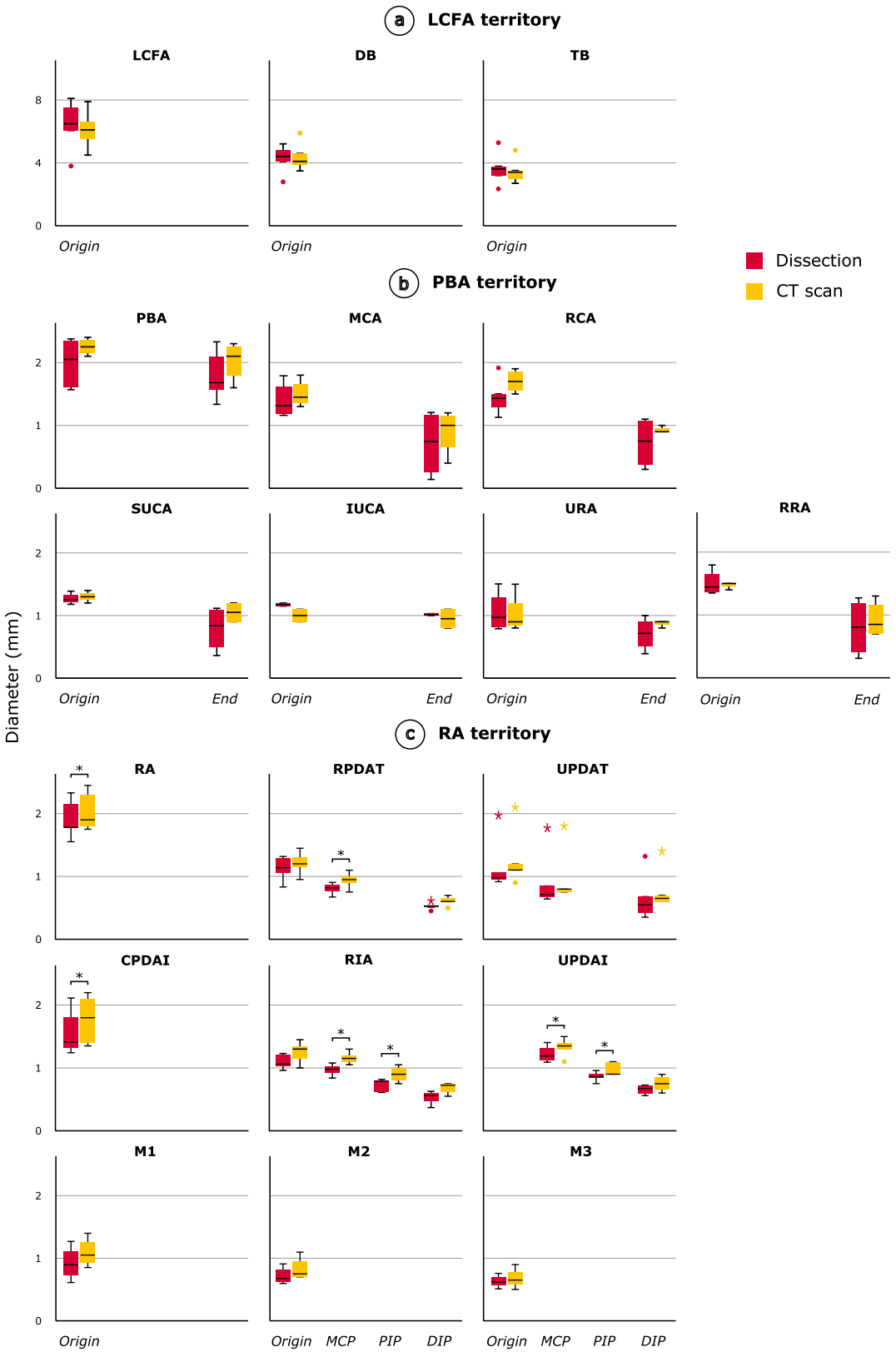

Fig. 6. Boxplots of artery diameter of the LCFA territory (a), the PBA territory (b), and the RA territory (c), and their comparison between dissection and CT scan measurements. LCFA: lateral circumflex femoral artery, DB: descending branch, TB: transverse branch, PBA: profunda brachii artery, MCA: medial collateral artery, RCA: radial collateral artery, RRA: radial recurrent artery, SUCA: superior ulnar collateral artery, IUCA: inferior ulnar collateral artery, URA: ulnar recurrent artery, RA: radial artery, RPDAT: radial palmar digital artery of the thumb, UPDAT: ulnar palmar digital artery of the thumb, CPDAI: common palmar digital artery of the index, RIA: radialis indicis artery, UPDAI: ulnar palmar digital artery of the index, M1: 1st metacarpal artery, M2: 2nd metacarpal artery, M3: 3rd metacarpal artery, MCP: metacarpophalangeal joint, PIP: proximal interphalangeal joint, DIP: distal interphalangeal joint. For the thumb arteries (RPDAT and UPDAT), the DIP joint localization corresponds to the interphalangeal (IP) joint. Yellow and red dots: outliers, yellow and red stars: extreme outliers, *: $p<0.05$.

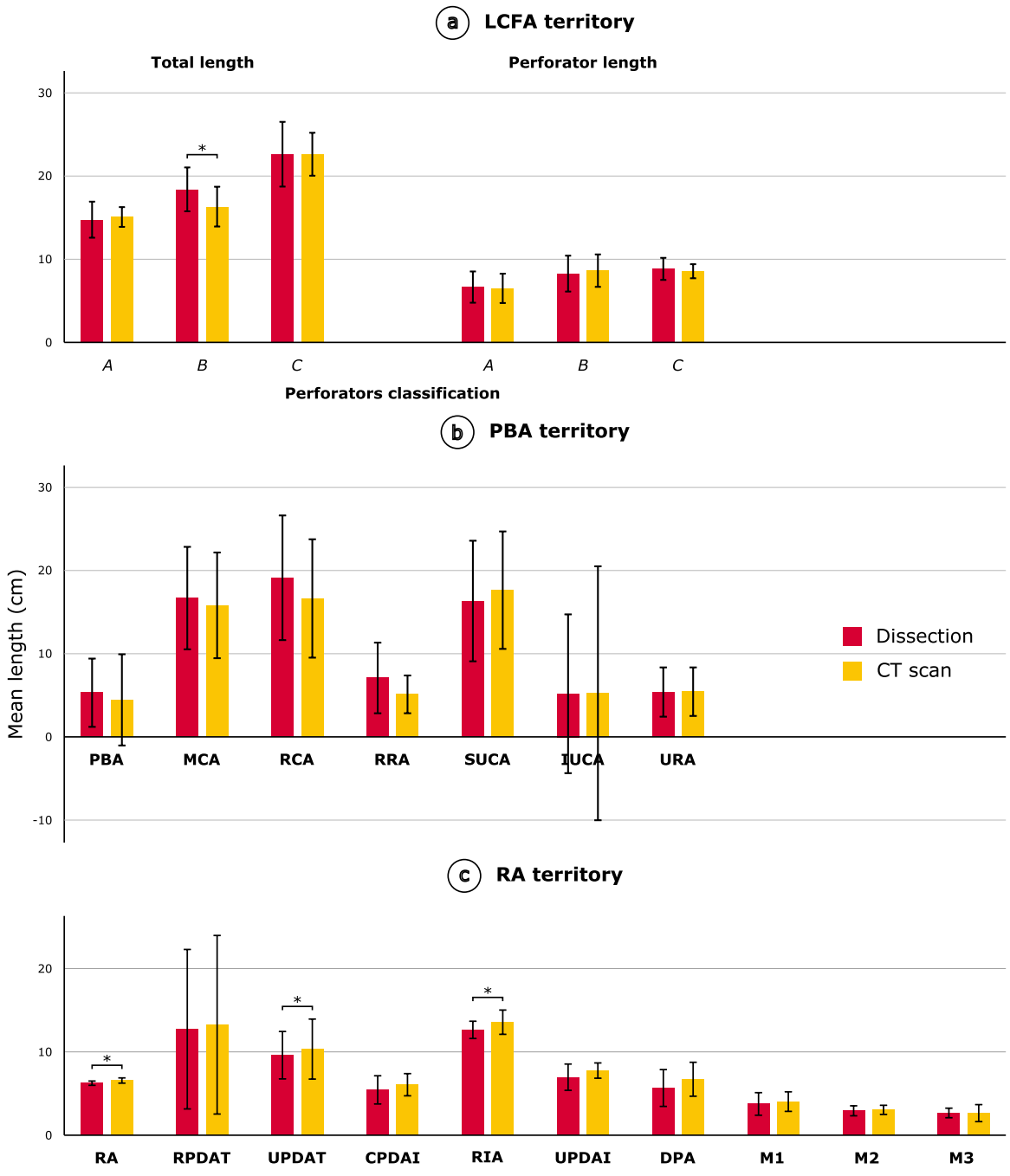

Fig. 7. Histograms of artery length of the LCFA territory (a), the PBA territory (b), and the RA territory (c), and their comparison between dissection and CT scan measurements. LCFA: lateral circumflex femoral artery, DB: descending branch, TB: transverse branch, PBA: profunda brachii artery, MCA: medial collateral artery, RCA: radial collateral artery, SUCA: superior ulnar collateral artery, RRA: radial recurrent artery, IUCA: inferior ulnar collateral artery, URA: ulnar recurrent artery, RA: radial artery, RPDAT: radial palmar digital artery of the thumb, UPDAT: ulnar palmar digital artery of the thumb, CPDAI: common palmar digital artery of the index, RIA: radialis indicis artery, UPDAI: ulnar palmar digital artery of the index, M1–2–3: 1st–2nd–3rd metacarpal arteries. Error bars: 95 % CI, *: $p<0.05$.

measurement modality, even for very small arteries, indicating a high level of precision of the injection. The comparison between the diameters in our study and the literature showed good similarities. For example, the ØRCA of 1.5 mm (range 1 – 3 mm, localization of measurement not specified) (Ninkovic and Dornseifer, 2009) was comparable to our $ØRCA_{origin}$ of 1.45 +/- 0.29 mm, or ØPBA of 2.05 +/- 0.16 mm (Przybycień et al., 2022), similar to our $ØPBA_{origin}$ of 1.99 +/- 0.39 mm.

A difference of length between dissection and CT scan might be due to artery tortuosity. Dissection permits the extension of the artery and a precise measure of its entire length. However, a CT scan is a more favorable approach for 3D visualization of arterial natural paths and waviness quantification. The tortuosity of structures like fibers was previously quantified with microCT (Leyssens et al., 2023; Maes et al., 2022; Manon et al., 2024). This quantification method could be implemented on vessels benefiting from the Angiofil-latex enlightenment on microCT or classical CT scans. While the software in this study did not permit unrolling of the vessels, specific software capable of this could be also considered for future work.

Even if an anatomical variation is not rare, and that small sample size is more sensitive to inter-individual anatomical variations, caution should be paid when comparing results with other studies. Some

meaningful variations were found in the literature. For example, a length of 4.97 +/- 1.96 cm was described for the MCA (Souza et al., 2010) whereas we obtained a MCA length of 16.7 +/- 3.9 cm. This difference came from the various landmarks. These authors measured the length from the MCA origin to its penetration into the lateral head of the triceps brachii. On the contrary, the artery was measured from its origin until its end, thus up to the first anastomosis with recurrent corresponding arteries. Another book chapter describing the lateral arm flap mentioned a RCA length of 6 cm (range 4 – 8 cm) (Ninkovic and Dornseifer, 2009) instead of our RCA length of 19.1 +/- 6.0 cm. In this case, the authors only considered the posterior branch of the RCA, not the whole RCA until its final anastomosis.

Therefore, variability and dispersion between CT scan and dissection measures, particularly the length, resulted from anatomical variations rather than the modality of measurement itself.

4.2. Angiofil and latex combination

Alone, the Angiofil can opacify capillaries of 15 μm (Grabherr et al., 2008a, 2008b). Compared to the Microfil (MV-122, Flow-Tech Inc.), a colored silicone rubber cast agent (Grabherr et al., 2008a, 2007) that allows the visualization of vessels less than 20 μm in diameter (Marxen et al., 2004), the Angiofil was proven to achieve the same performance (Grabherr et al., 2008a). However, the combination with latex changes the fluidity of the solution. The viscosity is directly related to the caliber of vessels that can be filled (Grabherr et al., 2008a, 2007). Compared to other cast materials, the fluidity of the latex facilitates penetration in the deep vasculature, allowing an excellent distribution in peripheral arteries (Alvernia et al., 2010; Renard et al., 2018). The hardening time of several days also enables the progressive pressure dispersion to tinier arterioles. However, it does not go through capillaries. The microcirculation or the venous network cannot be penetrated as with many other cast materials such as gelatine (Grabherr et al., 2007). One cast agent containing barium sulphate, called the Micropaque, could penetrate capillaries when dissolved into water but also leads to extravasation (Grabherr et al., 2007; Renard et al., 2018). The adjustable viscosity of the Angiofil, depending on the solvent choice and concentration (Grabherr et al., 2008a), permitted to reach arteries as small as 0.3 mm in diameter, even with a death-to-perfusion time extensively increased. This technique could still be used on fresh-frozen limbs, maintaining this precision, without considering the storage duration. The interval between the death and the injection could then be extended without altering outcomes. The absence of extravasation thanks to the hydrophobic characteristic and the fixation of Angiofil by latex solidification might allow a durable signal visualization (Hlushchuk et al., 2019). In addition, the CT scan signal of Angiofil was a bit lowered by the adjunction of latex, justifying to increase its concentration in the mixture compared to the literature (Grabherr et al., 2008a). The final resolution was only limited by the maximal resolution of the CT scan. The same injected tissues imaged by microCT could allow to precise the minimal vessel diameter this mixture can penetrate (Bernard et al., 2020; Hlushchuk et al., 2019). This imaging technique combined with the Angiofil injection could enable automated segmentation of the peripheral vascular network, at the level of perforators, and the extraction of quantitative data such as length and caliber (Grabherr et al., 2008a, 2008b; Hlushchuk et al., 2019). Otherwise, a venous retrograde injection could be considered to opacify the venous bed with the Angiofil-latex mixture, depending on valvular tightness.

The Angiofil-latex technique presents numerous advantages previously mentioned, particularly in terms of accessibility. To our knowledge, only one commercialized product gathers all the same advantages, the μAngiofil (Hlushchuk et al., 2019), which includes an Angiofil contrast agent and cast material based on a polyurethane resin. However, it is twenty times more expensive than the Angiofil for the same volume. The technique developed here appears much cheaper and more accessible to the researcher while providing the same benefits, and without additional difficulties.

Besides its visibility on the CT scan, the Angiofil is also apparent on magnetic resonance imaging (MRI) by its high fatty signal in T1-weighted sequence (Bruguier et al., 2015; Renard et al., 2018). The study could then be extended to MRI analyses to confirm that this technique might be used for three modalities in the same injection, *i.e.* the CT scan, the MRI, and the dissection.

In this study, the addition of Angiofil did not alter the inherent qualities of latex and despite a little contrast attenuation by the latex, increasing Angiofil concentration solved this potential issue. Finally, it provides a homogeneous mixture reaching very small arteries, which reaffirms the suitability of this combination as a valuable material for anatomical studies, especially those focused on the design of skin flaps which require precise data about perforator location and distribution, about pedicle caliber and length, and about distal anastomosing networks allowing the elevation of reversed flow flaps.

Those advantages also improve the identification of anatomical variations or anomalies in the vascular network, such as for the origin of UPDAT and RPDAT, supporting the debate in the literature about deleting the term of princeps pollicis artery (Gnanasekaran et al., 2022; Miletin et al., 2017). The anatomical nomenclature tends sometimes to differ between the different studies. This new technique could permit to clarify the standardization of anatomical nomenclature, routes, origins, and variations during further research with a larger sample size, in both modalities.

4.3. Pitfalls to avoid and recommendations

The quality of our observations using the single Angiofil-latex injection is based on three essential technical points of attention: rinsing, dissection, and system tightness.

First, a good rinse must remove all the blood clots, residue, and debris (Bergeron et al., 2006; Grabherr et al., 2007), ensuring the Angiofil-latex mixture flows smoothly and uniformly. Even if the CT scan has a high sensitivity to detect vascular lesions (Chevallier et al., 2013), arterial occlusion could be misinterpreted as lesions (Fig. 3a). The best way to proceed is to rinse the upstream artery to carefully preserve and ensure complete washing of the downstream network. Cleaning the vascular network with preheated 0.9 % NaCl solution reduces fluid viscosity, making vessel walls more pliable and minimizing mechanical resistance.

Secondly, all small collaterals must be carefully dissected and clamped. A coarse dissection before the rinse or the injection will inevitably lead to the rupture of small arterioles that are difficult to see with the naked eye. Any little gap in the vascular wall will further lead to an extravasation of the liquid, thereby decreasing the efficacy of the technique and compromising quantitative analyses (Fig. 3b). Therefore, a minimal invasive approach and a dissection *a minima* are strongly recommended during these two steps in order to preserve the vascular network, avoid leakage, and achieve optimal results. To avoid other sources of arterial damage, an appropriate size of catheter is required to proceed with a safe introduction, and a delicate continuous pressure will protect from the rupture risk due to potential overpressure. If an entire part of a limb or a single organ needs to be contrasted, another tip to estimate the injection volume and avoid overflows is to thaw the limb in a head-down position to bleed out and quantify the extracted blood.

Finally, the third pitfall to avoid is the intravascular air injection. Air bubbles can negatively impact the quality of the radiological outcomes, leading to artifacts, opacification skips (Fig. 3c) or obstruction and, potentially, to suboptimal results. Therefore, an airtight system is crucial during all the steps. A good preliminary rinse also helps to eliminate air bubbles, preventing artifacts and incomplete filling (Grabherr et al., 2007). Thus, this step is crucial for preparing vessels and achieving optimal vascular imaging and anatomical analysis.

5. Conclusions

This new combination of Angiofil-latex injection offers a simple, cheap, reliable, and non-toxic possibility to opacify, visualize, and enhance analyses of vascular networks. This association of a contrast agent and a vascular cast material in conjunction with an optimal rinse and injection, allows for clear and detailed visualization of not only large and small arteries vascularizing the deep muscular compartments of the limbs, but also the thin and very thin vessels supplying the overlying integuments.

The enhanced visibility of the vascular network in the CT scan can play a significant role in the preliminary planning of dissections, particularly because the radiological images offer different views and post-processing 3D reconstructions. This information helps in determining the most appropriate approach, guiding the dissection. The dissection is also improved by the rigidification and the color of the latex. The arteries can be identified by touch, like a solid cord, as well as by sight of the specific color used. The outcomes are fixed through latex solidification and can be stored in a freezer, enabling multiple reuses for iterative analyses. Taking advantage of this new method could lead to potential major impact on medical research, pathology or nomenclature description, forensic medicine, and education.

Ethical statement

Human cadaveric donors were received from the Human Anatomy Department of UCLouvain (IRB00008535, Brussels, Belgium). Distinct limbs were harvested for each vascular territory, following local ethics committee authorization (Ref 2021–30AOU-356, approved on the 13th of September 2021).

CRediT authorship contribution statement

Julie Manon: Writing – original draft, Visualization, Methodology, Investigation, Formal analysis, Conceptualization. **Gaspary Fodjeu:** Writing – original draft, Validation, Investigation, Formal analysis. **Robin Evrard:** Methodology, Investigation, Formal analysis, Conceptualization. **Lucien Van den Broeck:** Writing – original draft, Investigation, Formal analysis. **Mathieu Jacob:** Writing – original draft, Investigation, Formal analysis. **Emmanuel Coche:** Writing – review & editing, Supervision, Resources. **Olivier Cornu:** Writing – review & editing, Supervision, Funding acquisition. **Catherine Behets:** Writing – review & editing, Supervision, Resources. **Benoît Lengelé:** Writing – review & editing, Supervision, Resources.

Declaration of Competing Interest

The authors declare that they have no known competing financial interests or personal relationships that could have appeared to influence the work reported in this paper.

Data availability statement

All data analyzed during the study are included in this published article/Supplementary Data. The complete original datasets generated during the current study are available from the corresponding author on reasonable request.

Acknowledgments

The authors declare no conflict of interest. Fig. 2 was partly generated using templates provided by Servier Medical Art (http://smart.servier.com/, downloaded on 14 July 2022), licensed under a Creative Commons Attribution 3.0 unported license (https://creativecommons.org/licenses/by/3.0/, accessed on the 14 July 2022). The authors are grateful to all those who contributed to this work, including Lies Fievé, Xavier de Spiegeleire, Frédéric Delandmeter, Loïc Fonkoué, Bernard Caelen, Nicolas Charles-Pirlot, Michelle Cougnon, and Walter Hudders. Last but not least, the authors extend their deepest gratitude to the body donors and their families. The Christian Delloye's Fund made this research possible. Additionally, the F.S.R. Fund ("Fonds Spécial pour la Recherche," Belgium) and F.N.R.S. Aspirant Fund awarded to Dr. Julie MANON and Dr. Robin EVRARD ("Fonds National de la Recherche Scientifique", Application ID 40004991 and ID 40010491 respectively, Belgium) supported this research.

Appendices

Additional Table A
Comparison of artery diameters analyzed by CT scan and dissection

Artery	*Localization*	*Dissection (mm) (mean +/- SD)*	*CT scan (mm) (mean +/- SD)*	*P-value*
LCFA territory				
LCFA	Origin	6.40 +/- 1.66	6.12 +/- 1.27	.345
	DB	4.27 +/- 0.92	4.40 +/- 0.93	.684
	TB	3.64 +/- 1.07	3.48 +/- 0.80	.500
PBA territory				
PBA	Origin	1.99 +/- 0.39	2.25 +/- 0.13	.273
	End	1.80 +/- 0.40	2.03 +/- 0.31	.715
MCA	Origin	1.40 +/- 0.29	1.50 +/- 0.22	.068
	End	0.71 +/- 0.53	0.90 +/- 0.36	.465
RCA	Origin	1.45 +/- 0.29	1.70 +/- 0.18	.465
	End	0.73 +/- 0.41	0.93 +/- 0.05	.465
SUCA	Origin	1.27 +/- 0.09	1.30 +/- 0.08	.465
	End	0.79 +/- 0.36	1.05 +/- 0.17	.068
RRA	Origin	1.51 +/- 0.20	1.48 +/- 0.05	1.000
	End	0.80 +/- 0.46	0.93 +/- 0.28	.273
IUCA	Origin	1.18 +/- 0.04	1.00 +/- 0.14	.180
	End	1.02 +/- 0.04	0.95 +/- 0.21	.655
URA	Origin	1.06 +/- 0.32	1.03 +/- 0.32	.465
	End	0.71 +/- 0.26	0.88 +/- 0.05	.197
RA territory				

(*continued on next page*)

Additional Table A (*continued*)

Artery	*Localization*	*Dissection (mm) (mean +/- SD)*	*CT scan (mm) (mean +/- SD)*	*P-value*
RA	Origin	1.92 +/- 0.32	2.04 +/- 0.32	**.043**
RPDAT	Origin	1.13 +/- 0.20	1.21 +/- 0.19	.345
	MCP	0.80 +/- 0.09	0.94 +/- 0.13	**.043**
	IP	0.53 +/- 0.06	0.61 +/- 0.07	.080
UPDAT	Origin	1.18 +/- 0.45	1.28 +/- 0.47	.080
	MCP	0.93 +/- 0.48	0.98 +/- 0.46	.138
	IP	0.66 +/- 0.39	0.79 +/- 0.34	.104
CPDAI	Origin	1.58 +/- 0.37	1.77 +/- 0.39	**.043**
RIA	Origin	1.10 +/- 0.12	1.25 +/- 0.18	.080
	MCP	0.97 +/- 0.09	1.16 +/- 0.10	**.043**
	PIP	0.73 +/- 0.10	0.90 +/- 0.13	**.043**
	DIP	0.53 +/- 0.11	0.69 +/- 0.09	.068
UPDAI	MCP	1.23 +/- 0.13	1.33 +/- 0.15	**.043**
	PIP	0.87 +/- 0.08	0.98 +/- 0.11	**.043**
	DIP	0.66 +/- 0.08	0.75 +/- 0.13	.144
M1	Origin	0.92 +/- 0.27	1.09 +/- 0.23	.068
M2	Origin	0.71 +/- 0.14	0.83 +/- 0.19	.144
M3	Origin	0.63 +/- 0.13	0.68 +/- 0.20	.276

SD: standard deviation, LCFA: lateral circumflex femoral artery, DB: descending branch, TB: transverse branch, PBA: profunda brachii artery, MCA: medial collateral artery, RCA: radial collateral artery, SUCA: superior ulnar collateral artery, RRA: radial recurrent artery, IUCA: inferior ulnar collateral artery, URA: ulnar recurrent artery, RA: radial artery, RPDAT: radial palmar digital artery of the thumb, UPDAT: ulnar palmar digital artery of the thumb, CPDAI: common palmar digital artery of the index, RIA: radialis indicis artery, UPDAI: ulnar palmar digital artery of the index, M1–2–3: 1st–2nd–3rd metacarpal arteries.

Additional Table B
Comparison of artery lengths analyzed by CT scan and dissection

Length	*Artery*	*Dissection (cm) (mean +/- SD)*	*CT scan (cm) (mean +/- SD)*	*P-value*
LCFA territory				
Total	A	14.8 +/- 3.6	15.1 +/- 2.0	.196
	B	18.4 +/- 4.1	16.3 +/- 3.8	**.010**
	C	22.6 +/- 5.8	22.6 +/- 3.8	.722
Perforator	A	6.6 +/- 3.1	6.5 +/- 2.9	.780
	B	8.3 +/- 3.4	8.6 +/- 3.1	.212
	C	8.8 +/- 2.0	8.6 +/- 1.3	.754
PBA territory				
Total	PBA	5.3 +/- 3.3	4.5 +/- 3.4	.144
	MCA	16.7 +/- 3.9	15.8 +/- 4.0	.068
	RCA	19.1 +/- 6.0	16.6 +/- 4.5	.197
	RRA	7.1 +/- 2.7	5.1 +/- 1.4	.068
	SUCA	16.3 +/- 4.6	17.6 +/- 4.4	.068
	IUCA	5.3 +/- 1.1	5.2 +/- 1.7	.655
	URA	5.4 +/- 1.9	5.4 +/- 1.8	.715
RA territory				
Total	RA	6.2 +/- 0.2	6.6 +/ 0.2	**.042**
	RPDAT	12.7 +/- 7.7	13.3 +/- 8.6	.233
	UPDAT	9.6 +/- 2.3	10.3 +/- 2.9	**.043**
	CPDAI	5.4 +/- 1.4	6.1 +/- 1.1	.080
	RIA	12.6 +/- 0.8	13.6 +/- 1.2	**.043**
	UPDAI	7.0 +/- 1.3	7.8 +/- 0.7	.068
	DPA	5.7 +/- 1.4	6.7 +/- 1.3	.068
	M1	3.8 +/- 0.9	4.0 +/- 0.7	.068
	M2	2.9 +/- 0.4	3.0 +/- 0.3	.144
	M3	2.7 +/- 0.2	2.6 +/- 0.4	1.000

SD: standard deviation, LCFA: lateral circumflex femoral artery, A, B and C: Perforation classification according to Yu et al. (Yu, 2004), PBA: profunda brachii artery, MCA: medial collateral artery, RCA: radial collateral artery, RRA: radial recurrent artery, SUCA: superior ulnar collateral artery, IUCA: inferior ulnar collateral artery, URA: ulnar recurrent artery, RA: radial artery, RPDAT: radial palmar digital artery of the thumb, UPDAT: ulnar palmar digital artery of the thumb, CPDAI: common palmar digital artery of the index, RIA: radialis indicis artery, UPDAI: ulnar palmar digital artery of the index, DPA: deep palmar arch, M1-2–3: 1st–2nd–3rd metacarpal arteries.

References

Alvernia, J.E., Pradilla, G., Mertens, P., Lanzino, G., Tamargo, R.J., 2010. Latex injection of cadaver heads: technical note. Neurosurgery 67, 362–367.

Atasoy, E., IOAKIMIDIS, E., KASDAN, M.L., KUTZ, J.E., KLEINERT, H.E., 1970. Reconstruction of the amputated finger tip with a triangular volar flap: A new surgical procedure. JBJS 52, 921–926.

Bergeron, L., Tang, M., Morris, S.F., 2006. A review of vascular injection techniques for the study of perforator flaps. Plast. Reconstr. Surg. 117, 2050–2057.

Bernard, F., Mercier, P., Chappard, D., 2020. Microvascularization of the human central and peripheral nervous system: A new microcomputed tomography method. Morphologie 104, 247–253.

Boyd, B., Zamora, C.A., Castillo, M., 2017. Managing Adverse Reactions to Contrast Agents. Magn. Reson Imaging Clin. N. Am. 25, 737–742.

Bruen, R., Stirling, A., Ryan, M., Sheehan, M., MacMahon, P., 2022. Shelling the myth: allergies to Iodine containing substances and risk of reaction to Iodinated contrast media. Emerg. Radio. 29, 67–73.

Bruguier, C., Egger, C., Vallée, J.P., Grimm, J., Boulanger, X., Jackowski, C., Mangin, P., Grabherr, S., 2015. Postmortem magnetic resonance imaging of the heart ex situ: development of technical protocols. Int J. Leg. Med 129, 559–567.
Catalano, L.W., Zlotolow, D.A., Hitchcock, P.B., Shah, S.N., Barron, O.A., 2011. Surgical exposures of the radius and ulna. J. Am. Acad. Orthop. Surg. 19, 430–438.
Chevallier, C., Doenz, F., Vaucher, P., Palmiere, C., Dominguez, A., Binaghi, S., Mangin, P., Grabherr, S., 2013. Postmortem computed tomography angiography vs. conventional autopsy: advantages and inconveniences of each method. Int J. Leg. Med 127, 981–989.
Dappa, E., Higashigaito, K., Fornaro, J., Leschka, S., Wildermuth, S., Alkadhi, H., 2016. Cinematic rendering – an alternative to volume rendering for 3D computed tomography imaging. Insights Imaging 7, 849–856.
Evrard, R., Manon, J., Rafferty, C., Fieve, L., Cornu, O., Kirchgesner, T., Lecouvet, F.E., Schubert, T., Lengele, B., 2024. Vascular study of decellularized porcine long bones: Characterization of a tissue engineering model. Bone 182, 117073.
Fonkoue, L., Behets, C., Steyaert, A., Kouassi, J.K., Detrembleur, C., Cornu, O., 2021. Anatomical study of the descending genicular artery and implications for IMAGE-GUIDED interventions for knee pain. Clin. Anat. 34, 634–643.
Gnanasekaran, D., Veeramani, R., Karuppusamy, A., 2022. Reappraisal of arterial anatomy of thumb. Anat. Cell Biol. 55, 414–422.
Grabherr, S., Djonov, V., Yen, K., Thali, M.J., Dirnhofer, R., 2007. Postmortem angiography: review of former and current methods. AJR. Am. J. Roentgenol. 188, 832–838.
Grabherr, S., Hess, A., Karolczak, M., Thali, M.J., Friess, S.D., Kalender, W.A., Dirnhofer, R., Djonov, V., 2008b. Angiofil-mediated visualization of the vascular system by microcomputed tomography: a feasibility study. Microsc. Res Tech. 71, 551–556.
Grabherr, S., Dominietto, M., Yu, L., Djonov, V., Müller, B., Friess, S., 2008a. Angiofil: a novel radio-contrast agent for post-mortem micro-angiography. In: Stock, S.R. (Ed.),. Presented at the Optical Engineering + Applications, San Diego, California, USA, p. 70781 O.
Grabherr, S., Grimm, J., Dominguez, A., Vanhaebost, J., Mangin, P., 2014. Advances in post-mortem CT-angiography. Br. J. Radiol. 87.
Hlushchuk, R., Haberthür, D., Djonov, V., 2019. Ex vivo microangioCT: Advances in microvascular imaging. Vasc. Pharmacol. 112, 2–7.
Jackowski, C., Persson, A., Thali, M.J., 2008. Whole body postmortem angiography with a high viscosity contrast agent solution using poly ethylene glycol as contrast agent dissolver. J. Forensic Sci. 53, 465–468.
Lee, Y.-C., Chen, W.-C., Chou, T.-M., Shieh, S.-J., 2015. Anatomical Variability of the Anterolateral Thigh Flap Perforators: Vascular Anatomy and Its Clinical Implications. Plast. Reconstr. Surg. 135, 1097–1107.
Leyssens, L., Balcaen, T., Pétré, M., Béjar Ayllón, N., El Aazmani, W., De Pierpont, A., Pyka, G., Lacroix, V., Kerckhofs, G., 2023. Non-destructive 3D characterization of the blood vessel wall microstructure in different species and blood vessel types using contrast-enhanced microCT and comparison with synthetic vascular grafts. Acta Biomater. 164, 303–316.
Littler, J.W., 1953. The neurovascular pedicle method of digital transposition for reconstruction of the thumb. Plast. Reconstr. Surg. 12, 303–319.
Maes, A., Pestiaux, C., Marino, A., Balcaen, T., Leyssens, L., Vangrunderbeeck, S., Pyka, G., De Borggraeve, W.M., Bertrand, L., Beauloye, C., Horman, S., Wevers, M., Kerckhofs, G., 2022. Cryogenic contrast-enhanced microCT enables nondestructive 3D quantitative histopathology of soft biological tissues. Nat. Commun. 13, 6207.
Manon, J., Evrard, R., Maistriaux, L., Fievé, L., Heller, U., Magnin, D., Boisson, J., Kadlub, N., Schubert, T., Lengelé, B., Behets, C., Cornu, O., 2022. Periosteum and fascia lata: Are they so different? Front. Bioeng. Biotechnol. 10, 944828.
Manon, J., Evrard, R., Fievé, L., Bouzin, C., Magnin, D., Xhema, D., Darius, T., Bonaccorsi-Riani, E., Gianello, P., Docquier, P.-L., Schubert, T., Lengelé, B., Behets, C., Cornu, O., 2023. A New Osteogenic Membrane to Enhance Bone Healing: At the Crossroads between the Periosteum, the Induced Membrane, and the Diamond Concept. Bioengineering 10, 143.
Manon, J., Gallant, L., Gérard, P., Fieve, L., Schneidewind, P., Pyka, G., Kerckhofs, G., Lengelé, B., Cornu, O., Behets, C., 2024. 2D and 3D microstructural analysis of the iliotibial tract. Journal of Anatomy In review.
Marxen, M., Thornton, M.M., Chiarot, C.B., Klement, G., Koprivnikar, J., Sled, J.G., Henkelman, R.M., 2004. MicroCT scanner performance and considerations for vascular specimen imaging. Med. Phys. 31, 305–313.
Miletin, J., Sukop, A., Baca, V., Kachlik, D., 2017. Arterial supply of the thumb: Systemic review. Clin. Anat. 30, 963–973.
Ninkovic, M., Dornseifer, U., 2009. Lateral arm flap. In: Flaps and Reconstructive Surgery. Elsevier, pp. 305–319.
Park, H., Kim, D.-J., Hwang, J., 2021. Reconstruction of a Mangled Hand with a Thoracodorsal Artery Perforator Free Flap: A Report of Two Cases. Arch. Hand Microsurg. 26.
Protopsaltis, T.S., Ruch, D.S., 2008. Volar approach to distal radius fractures. J. Hand Surg. Am. 33, 958–965.
Przybycień, W., Bonczar, M., Ostrowski, P., Koziej, M., Mizia, E., Wysiadecki, G., Loukas, M., Walocha, J., 2022. The deep brachial artery—A meta-analysis of its origin and diameter with a review of the literature. Clin. Anat. 35, 838–846.
Renard, Y., Hossu, G., Chen, B., Krebs, M., Labrousse, M., Perez, M., 2018. A guide for effective anatomical vascularization studies: useful ex vivo methods for both CT and MRI imaging before dissection. J. Anat. 232, 15–25.
Rosado Ingelmo, A., Doña Diaz, I., Cabañas Moreno, R., Moya Quesada, M.C., García-Avilés, C., García Nuñez, I., Martínez Tadeo, J.I., Mielgo Ballesteros, R., Ortega-Rodríguez, N., Padial Vilchez, M.A., Sánchez-Morillas, L., Vila Albelda, C., Moreno Rodilla, E., Torres Jaén, M.J., 2016. Clinical Practice Guidelines for Diagnosis and Management of Hypersensitivity Reactions to Contrast Media. J. Invest. Allergol. Clin. Immunol. 26, 144–155 quiz 2 p following 155.
Saint-Cyr, M., Oni, G., Lee, M., Yi, C., Colohon, S.M., 2012. Simple Approach to Harvest of the Anterolateral Thigh Flap. Plast. Reconstr. Surg. 129, 207–211.
Salmon, M., 1936. Artères de la peau. In: Arteres de La Peau. pp. 246–246.
Souza, F.I. de, Saito, M., Torres, L.R., Wei, T.H., Mattar Junior, R., Zumiotti, A.V., 2010. Anatomic study of lateral arm flap with retrograde flow. Acta Ortop. Bras. 18, 39–43.
de Spiegeleire, X., Vanhaebost, J., Coche, E., 2019. Post-mortem CT angiography of mesenteric vessels using cinematic rendering vision. Diagn. Interv. Imaging 100, 533–534.
Stumm, C.J.-P., Wittig, H., Kalberer, N.M., Scheurer, E., 2020. Histomorphological assessment of isolated abdominal organs after targeted perfusion with the contrast agent Angiofil® in postmortem computed tomography angiography. Forensic Sci. Int. 315, 110427–110427.
Taylor, G.I., Corlett, R.J., Ashton, M.W., 2017. The Functional Angiosome: Clinical Implications of the Anatomical Concept. Plast. Reconstr. Surg. 140, 721–733.
Taylor, I.G., Pan, W.R., 1998. Angiosomes of the Leg: Anatomic Study and Clinical Implications. Plast. Reconstr. Surg. 102, 599.
Yu, P., 2004. Characteristics of the anterolateral thigh flap in a Western population and its application in head and neck reconstruction. Head. Neck 26, 759–769.